The Journal of Experimental Biology 210, 2231-2243
Published by The Company of Biologists 2007
doi:10.1242/jeb.001578

Death by small forces: a fracture and fatigue analysis of wave-swept macroalgae

Katharine J. Mach[1,*], Benjamin B. Hale[1], Mark W. Denny[1] and Drew V. Nelson[2]

[1]*Hopkins Marine Station of Stanford University, Pacific Grove, CA 93950, USA and* [2]*Department of Mechanical Engineering, Stanford University, Stanford, CA 94305, USA*

*Author for correspondence (e-mail: mach@stanford.edu)

Accepted 8 April 2007

Summary

Wave-swept macroalgae are subjected to large hydrodynamic forces as each wave breaks on shore, loads that are repeated thousands of times per day. Previous studies have shown that macroalgae can easily withstand isolated impositions of maximal field forces. Nonetheless, macroalgae break frequently. Here we investigate the possibility that repeated loading by sub-lethal forces can eventually cause fracture by fatigue. We determine fracture toughness, in the form of critical strain energy release rate, for several flat-bladed macroalgae, thereby assessing their resistance to complete fracture in the presence of cracks. Critical energy release rates are evaluated through single-edge-notch, pull-to-break tests and single-edge-notch, repeated-loading tests. Crack growth at sub-critical energy release rates is measured in repeated-loading tests, providing a first assessment of algal breakage under conditions of repeated loading. We then estimate the number of imposed waves required for un-notched algal blades to reach the point of complete fracture. We find that, if not checked by repair, fatigue crack growth from repeated sub-lethal stresses may completely fracture individuals within days. Our results suggest that fatigue may play an important role in macroalgal breakage.

Key words: fracture mechanics, macroalgae, seaweed, fatigue, breakage.

Introduction

As sessile organisms, intertidal macroalgae experience the full brunt of wave-induced water velocities, which in breaking waves commonly exceed 10 m s^{-1}. Hydrodynamic forces thereby imposed on seaweeds (Gaylord, 2000; Denny and Gaylord, 2002) are repeated for each of the more than 8000 waves impinging on shore each day. Despite its harshness, the wave-swept environment is home to some of Earth's most diverse and productive assemblages of organisms (Smith and Kinsey, 1976; Connell, 1978; Leigh et al., 1987). Accounting for such rich diversity in the midst of physical adversity is one of the central goals of intertidal ecomechanics.

To that end, studies of macroalgal material properties and morphological attributes have elucidated ways by which intertidal seaweeds withstand wave-imposed forces (e.g. Carrington, 1990; Holbrook et al., 1991; Denny and Gaylord, 2002; Pratt and Johnson, 2002; Kitzes and Denny, 2005; Martone, 2006). Although wave-induced flows potentially result in a variety of hydrodynamic forces (such as lift, acceleration reaction and impingement force), the bulk of hydrodynamic force for most seaweeds can be approximated as drag, which imposes tension on algal thalli (Gaylord et al., 1994; Gaylord, 2000; Gaylord et al., 2001). Most studies have thus examined breakage of seaweeds through pull-to-break tensile tests, which mimic imposition of drag force by a single wave. Strengths measured in tensile tests are often much greater than predicted maximal stresses encountered in the field (e.g. Koehl and Alberte, 1988; Gaylord et al., 1994; Gaylord, 2000; Johnson and Koehl, 1994; Friedland and Denny, 1995; Utter and Denny, 1996; Denny et al., 1997; Johnson, 2001; Kitzes and Denny, 2005), indicating that wave-swept macroalgae may be over-designed for resisting wave forces. The consequent low risk of breakage and dislodgment may help explain extant algal diversity (Denny, 2006). However, these conclusions must be viewed with skepticism. Contrary to prediction, large fractions of many algal populations are broken and dislodged each season (Seymour et al., 1989; Dudgeon and Johnson, 1992; Dudgeon et al., 1999; Johnson, 2001; Pratt and Johnson, 2002). How, then, can we reconcile our mechanical predictions with field observations?

Several factors, such as herbivory, abrasion, senescence and fatigue, have been suggested to increase breakage rates beyond those calculated for maximal hydrodynamic forces (Friedland and Denny, 1995; Utter and Denny, 1996; Kitzes and Denny, 2005; Denny, 2006). The action of these phenomena could bring predicted rates of breakage more in line with observations. As a first step towards evaluating these factors, we explore the role of fatigue, asking a fundamental question: does repeated loading of seaweeds lead to their breakage when single loadings do not?

Repeated force imposition may break seaweeds through several scenarios. First, repeated loading by waves may cause small fatigue cracks to form (Koehl, 1984; Koehl, 1986; Kitzes and Denny, 2005). The presence of such cracks – in addition to any cuts or nicks formed through abrasion or herbivory – reduces breaking strength (the stress that algae can resist before fracturing in two), thereby increasing the probability of breakage by large forces (e.g. Black, 1976; Johnson and Mann, 1986; Armstrong, 1987; Biedka et al., 1987; Denny et al., 1989; Lowell et al., 1991; DeWreede et al., 1992). Furthermore, once cracks are present (regardless of their source), repeated loading may cause them to grow until the alga breaks, even when algae are subjected only to small forces. Our goal here is to characterize the effects of cracks and the speeds with which they grow.

Fortunately, this inquiry into the potential role of algal fatigue can be guided by a robust engineering literature on formation and growth of cracks under repeated loading (e.g. Broek, 1982; Meguid, 1989; Janssen et al., 2004). Here we apply fracture mechanics techniques to assess crack growth in four intertidal and shallow subtidal macroalgae with flat-bladed morphologies. In the field, these algae may break at blade, stipe, and holdfast regions, but in this study, we focus on breakage of blades. We evaluate the fracture toughness of these macroalgae, assessing their resistance to complete fracture in the presence of cracks. We then measure crack growth in conditions of cyclic repeated loading, ultimately determining the number of imposed waves required for small cracks to grow to the point of complete fracture. See the accompanying article (Mach et al., 2007) for an extended description of fracture mechanics parameters and techniques.

In this study, we focus our attention on the tensile stresses in algae with flat-bladed morphologies, but fracture mechanics can also be applied to more complex algal structures, such as holdfasts or stiff, large-diameter stipes, which experience a variety of stresses. For such structures, finite element computer models previously developed for elastomeric components can be used to assess fatigue crack growth due to the combined effects of tensile, bending and shear stresses (Busfield et al., 2005).

Materials and methods

Specimens

Mazzaella flaccida (Setchell & Gardner) Fredericq was collected from intertidal rocks at Carmel River Beach in Carmel by the Sea, CA, USA, and Hopkins Marine Station in Pacific Grove, CA, USA. *Porphyra occidentalis* Setchell & Hus and *Mazzaella splendens* (Setchell & Gardner) Fredericq were collected at subtidal depths of 3–9 m at Carmel River Beach. *Ulva expansa* (Setchell) Setchell & Gardner was collected from floating docks in Monterey, CA, USA. The flat-bladed morphologies of these macroalgae facilitated observation of crack growth in conditions of repeated loading.

Testing apparatus

All tests were performed using a hydraulically driven tensometer, the driving arm (Parker Electrohydraulics, Elyria, OH, USA, PLA series) of which has positional accuracy of 51 μm. A 0–10 V signal from a 16-bit input/output board (National Instruments Corporation, Austin, TX, USA, model AT-MIO-16X) regulated the position of the driving arm, controlled through an interface written in LabVIEW (National Instruments Corporation).

Extension of test samples was determined from the position controller of the tensometer's actuator, an appropriate method because samples were thin blades tested at low stress with no observed slippage from sample grips. Engineering strain, ϵ, in the bulk of a specimen was computed as change in specimen length divided by initial length.

Force exerted on samples was measured using a waterproofed cantilever-style force transducer milled from an aluminum block. Four strain gauges (Measurements Group Inc., Raleigh, NC, USA, model CEA-13-062UW-350) were attached to the cantilever base in a full Wheatstone-bridge configuration. Force measurement accuracy was 0.005 N. Stress in the bulk of a specimen was defined as applied force divided by initial specimen cross-sectional area.

Samples were gripped by the tensometer as follows: thin strips of rubber were glued across algal sample ends with cyanoacrylate glue, and the tensometer grips were affixed to these rubber strips. Cyanoacrylate glue adhered well to all materials with no observed slippage. During loading, the rubber strips deformed a very small amount, but an analysis of this deformation showed it to have negligible effect on measurements of specimen extension.

Crack length in samples was measured using a telemicroscope (Questar Corporation, New Hope, PA, USA) fitted with an ocular Filar micrometer, the accuracy of which is 5 μm.

Single-edge-notch, pull-to-break tests

Critical strain energy release rate, T_C, quantifies strain energy release associated with crack propagation in a material [for an extended description, see accompanying article (Mach et al., 2007)]. T_C was determined from pull-to-break tests of single-edge-notch specimens of *M. flaccida*, *U. expansa* and *P. occidentalis*. Specimens cut from blades varied in length from approximately 7 to 11 cm and in width from approximately 0.9 to 1.7 cm. Samples were either left un-notched or given a notch of length ranging from 0.4 to 2.5 mm, with notches introduced as small razor-blade cuts perpendicular to one of a sample's long edges. *M. flaccida* and *P. occidentalis* were pulled until failure at a strain rate of approximately 0.2 s^{-1}, while *U. expansa* was extended to failure at a strain rate of 0.1 s^{-1}. *P. occidentalis* and *U. expansa* samples were submerged in seawater during tearing, while *M. flaccida* test pieces were wetted but not submerged.

For notched specimens, we made two calculations of critical strain energy release rate (Rivlin and Thomas, 1953; Lake, 1983) [see Eqn 9 in accompanying article (Mach et al., 2007)]. First, we calculated $T_{C,T}$:

$$T_{C,T} = (2\pi W_{o,T} a) / (\sqrt{1+\epsilon_{br}}) . \quad (1)$$

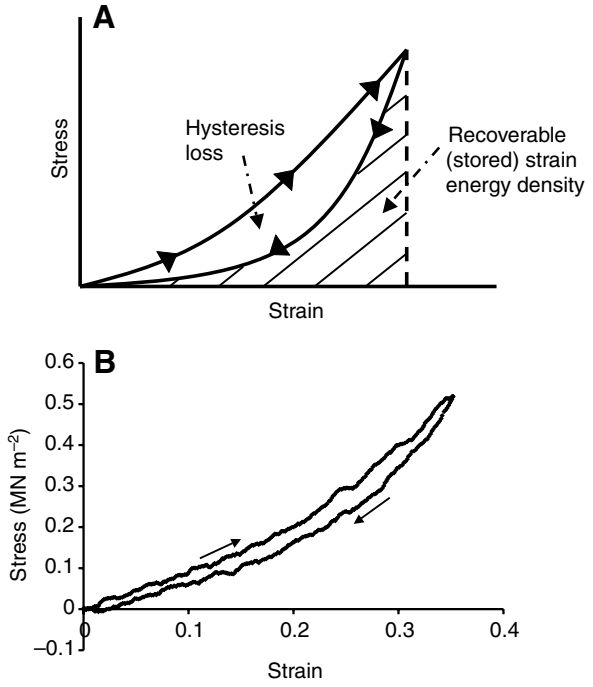

Fig. 1. (A) Example stress–strain curves for extension and retraction. Internal energy dissipation occurs as indicated by the hysteresis loss, the difference between input energy density and recoverable (stored) strain energy density. Input energy density is found as the area under the extension curve, while stored strain energy density is the hatched area under the retraction curve. (B) Loading of a *M. flaccida* specimen to maximum strain of approximately 0.35 demonstrates hysteretic loss.

$W_{o,T}$ is the total strain energy density absorbed by samples before fracture, ϵ_{br} is strain at breaking, and a is crack length in the specimen, the length of the introduced notch. The subscript 'T' indicates *total* strain energy density, the subscript 'C' indicates *critical* strain energy release rate, and the factor $\pi/\sqrt{1+\epsilon_{br}}$ is the appropriate value for k in eqn 9 in the accompanying article (Mach et al., 2007).

Eqn 1 is derived assuming elastic stress–strain behavior with no energy dissipation. However, algal blades exhibit some internal energy dissipation, as demonstrated by the hysteresis loops shown in Fig. 1. It has been suggested (Ahagon et al., 1975; Kinloch and Young, 1983; Kadir and Thomas, 1984; Seldén, 1995) that Eqn 1 can be applied to materials that dissipate energy by assuming that the stored energy density available for crack extension is the recoverable energy density under the retraction curve, $W_{o,S}$, (Fig. 1) instead of the input energy density under the extension curve, $W_{o,T}$. We thus calculated critical strain energy release rate from $W_{o,S}$ as well:

$$T_{C,S} = (2\pi W_{o,S} a) / (\sqrt{1+\epsilon_{br}}) . \quad (2)$$

The subscript 'S' indicates *stored* strain energy density. When no energy is dissipated, the extension and retraction curves follow the same path, making $W_{o,S}$ equivalent to $W_{o,T}$.

The total strain energy density, $W_{o,T}$, absorbed by a material before fracture was measured directly as area under the material's stress–strain curve during extension to breaking. $W_{o,S}$, on the other hand, was calculated for Eqn 2 using estimates of R, the resilience at breaking strain, because retraction curves cannot be measured for samples extended to fracture:

$$W_{o,S} = W_{o,T} R . \quad (3)$$

Resilience is the ratio of area under a retraction curve (hatched area in Fig. 1A) to total area under the extension curve (hysteresis loss area plus hatched area in Fig. 1A) (Wainwright et al., 1976). Each species' resilience as a function of strain was estimated by cycling un-notched test pieces to increasing extensions (Fig. 2). Resilience as a function of strain, determined from these cyclic-test measurements (Fig. 2B), was then used to estimate resilience at breaking strain for each single-edge-notch, pull-to-break test.

For calculations of both critical energy release rates, $T_{C,T}$ and $T_{C,S}$, the inverse of crack length, a, was plotted against

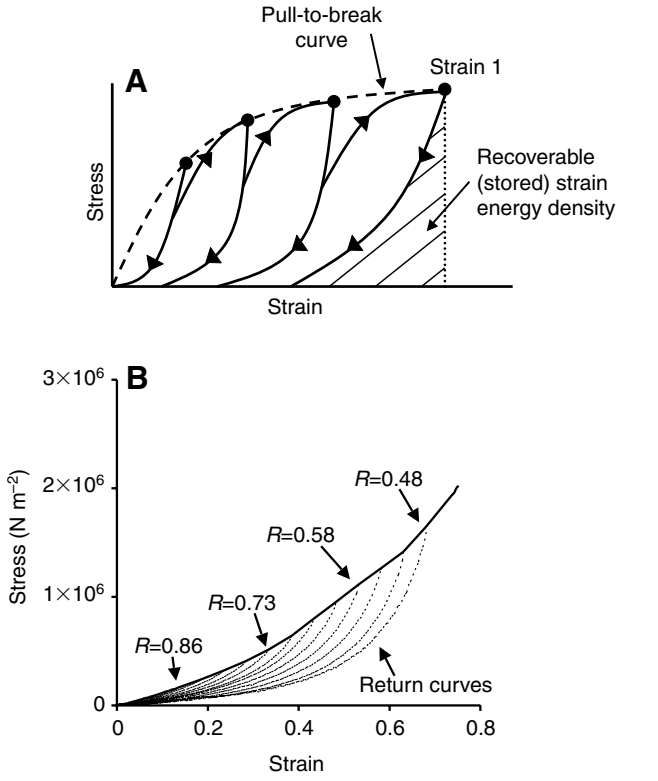

Fig. 2. (A) Schematic of stress–strain behavior observed when a specimen is cycled to increasingly larger strains. The tips of the extension–retraction loops trace a path that closely approximates the curve from a pull-to-break test. In this example, the pull-to-break curve is 'r-shaped'. Resilience at a strain level is taken as the ratio of area under the corresponding retraction curve to total area under the broken pull-to-break curve. For instance, for the strain level indicated by 'Strain 1', resilience is the ratio of the hatched area to the total area under the pull-to-break curve up to 'Strain 1'. (B) Experimental cycling behavior for *M. flaccida*. For clarity, only the retraction portions of loops (return curves) are shown. The bold line represents the reconstructed pull-to-break extension curve, which is gently 'J-shaped'. Resilience (R) at four strain levels is shown.

$(2\pi W_o)/(\sqrt{1+\epsilon_{br}})$, and the slope of the plot yielded critical energy release rate for total or stored strain energy density.

Many samples left un-notched broke at the grips due to tissue damage or stress concentrations introduced by the grips. These samples were removed from analysis. When an un-notched specimen – that is, a specimen without an intentionally introduced crack – broke at a location away from the grips, fracture was assumed to originate at a small, naturally occurring crack of unknown length a_o. Given that critical energy release rate $T_{C,S}$ is known from the single-edge-notch tests described above, a_o was estimated for an un-notched specimen by treating the assumed initial crack as an edge crack and solving for its length:

$$a_o = (T_{C,S}\sqrt{1+\epsilon_{br}}) / (2\pi W_{o,S}) . \quad (4)$$

Here, average $T_{C,S}$ for a species and estimated stored strain energy density, $W_{o,S}$, for each specimen at breakage were used.

Finally, for each species, critical strain energy release rate was expressed as:

$$T_{C,T} = (2\pi W_{o,T,\sigma} a) / (\sqrt{1+\epsilon_\sigma})$$

and

$$T_{C,S} = (2\pi W_{o,S,\sigma} a) / (\sqrt{1+\epsilon_\sigma}) , \quad (5)$$

where $T_{C,T}$ and $T_{C,S}$ are average critical strain energy release rates for each species; strain, ϵ_σ, is found as a function of applied stress, σ, from representative pull-to-break stress-strain curves for each species; total strain energy density as a function of applied stress, $W_{o,T,\sigma}$, is also calculated from representative stress-strain curves; and stored strain energy density as a function of stress, $W_{o,S,\sigma}$, is determined by applying Eqn 3. The subscript 'σ' indicates variables determined as fitted polynomial functions of applied stress. Breaking stress was determined for given crack lengths, a, by finding the values of stress, σ, that gave ϵ_σ and $W_{o,T,\sigma}$ (or ϵ_σ and $W_{o,S,\sigma}$) necessary to balance Eqn 5.

Crack propagation: single-edge-notch, repeated-loading tests

Single-edge-notch tests involving repeated cycling were performed on rectangular test pieces with lengths of 6.6–13.0 cm and widths of 1.4–3.1 cm. Sample sizes were constrained by the extent of flat and undamaged areas in blades of our test species. After samples were cut from blades, tissue adjacent to sites of future cracks was sectioned, and its thickness was determined using a compound microscope. Cross-sectional area of the test piece was calculated as the product of this approximately uniform thickness and the sample's width. All test pieces were immersed in cooled seawater during testing. For all tests, samples were cycled between zero strain and a fixed maximum cyclic strain. Cycling occurred at 1.0 Hz, with strain oscillating sinusoidally. Maximum imposed bulk strains ranged from 0.073 to 0.180, and maximum strain rates ranged from 0.23 s^{-1} to 0.57 s^{-1}.

Testing protocols were adapted from Seldén (Seldén, 1995), who describes standard methods for studying cyclic crack growth in rubber. Each test consisted of several phases. First, un-notched test pieces were conditioned by repeated cycling from zero strain to the test's maximum strain. When subjected to cyclic stretching, numerous elastomers and biological soft tissues experience the 'stress-softening' Mullins effect (Emery et al., 1997; Edsberg et al., 1999; Mars and Fatemi, 2004; Franceschini et al., 2006; Dorfmann et al., 2007), in which stress needed to reach a certain strain drops with each repeated cycle of stretching (e.g. Fig. 3). Conditioning prior to cyclic crack growth testing of rubber-like materials was suggested by Seldén (Seldén, 1995) to reduce the Mullins effect (Mullins, 1969), and experiment-appropriate conditioning of soft biological tissues has been

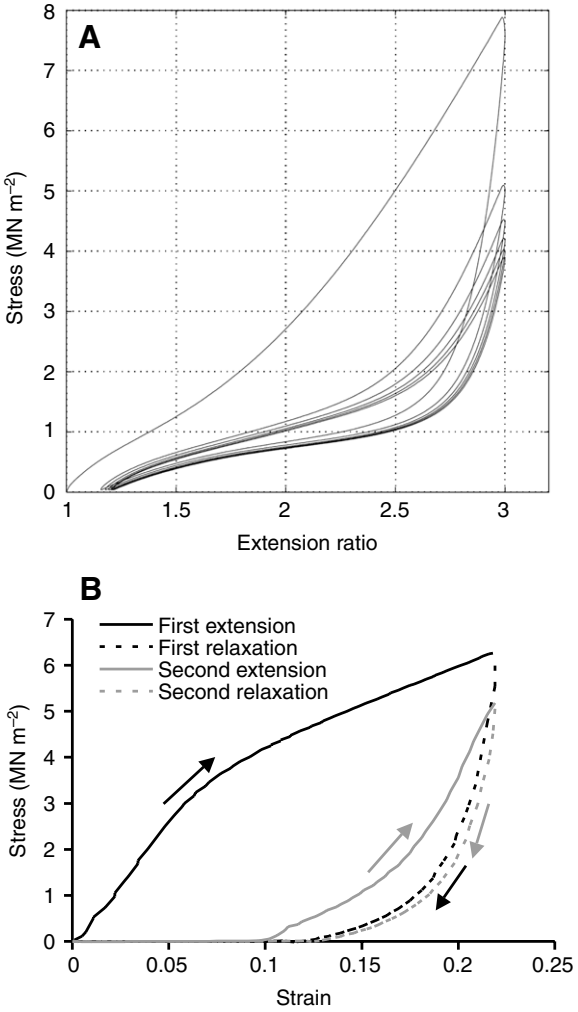

Fig. 3. (A) Conditioning of a particle-reinforced rubber specimen stretched to an extension ratio of 3. (Extension ratio is current specimen length divided by initial length.) The stress–strain curves, upon extension and retraction, exhibit 'stress softening', which is called the Mullins effect. This softening diminishes as the number of loading cycles increases. Plot is reprinted from Dorfmann and Ogden (Dorfmann and Ogden, 2004), copyright 2003, with permission from Elsevier. (B) Stress–strain curves of a brown alga, *Egregia menziesii* (Turner) Areschoug, for two cycles of extension and retraction. These curves also exhibit stress softening, with lower maximum stress reached in the second cycle. In addition, for both A and B, viscoelastic loading–unloading loops decrease in size with cycling.

found to reduce specimen- and test-related variability and to stabilize material behavior (Carew et al., 2004). Generally, stress softening diminishes after a sufficient number of constant-amplitude conditioning cycles, and stable stress–strain behavior ensues. If force–extension curves become uniform during conditioning, further changes in the force–extension curves can be assumed due to the soon-to-be introduced crack and not due to further stress relaxation.

Even after 2000–5000 conditioning cycles, algal blades demonstrated a slight, but measurable, decrease in stress that we considered in subsequent calculations. For each un-notched test piece during conditioning, maximum stored strain energy density per cycle, $W_{o,S}$, was measured as the area under the test piece's stress–strain curve during return from maximum strain to zero strain. To account for the continued relaxation observed in test specimens, $W_{o,S}$ was determined as a function of cycle number, N, during conditioning cycles for each sample. $W_{o,S}$ decreased as a logarithmic function of N:

$$W_{o,S}(N) = C_1 \log(N) + C_2 , \quad (6)$$

where C_1 and C_2 are constants fitted to experimental data. A linear regression of $\log(N)$ and strain energy density, $W_{o,S}$, was calculated to determine C_1 and C_2 for each sample, with the first 100 conditioning cycles excluded from the regression analysis to best estimate continued decreases in strain energy density after the initial steep drop. This equation was used for subsequent cycles to determine cycle-specific stored strain energy density for each sample.

After conditioning cycles were complete, enough seawater was drained from the tank to make a single edge notch of 0.5–3 mm perpendicular to a long edge of the test specimen. The initial length of the cut was determined by straining the sample slowly at 0.005 s^{-1} until the crack opened wide enough to be visible. A wet glass coverslip was placed on the back of the algal blade to ensure the region around the crack was flat and perpendicular to the telemicroscope, which was then used to measure crack length. Following this measurement, the coverslip was removed, seawater was replaced, and the notched sample was again cycled at 1.0 Hz between zero and maximum strain. After 500–1000 cycles, the tank was drained enough to expose the sample to air, and crack length was again measured. This procedure was repeated until the crack had grown in length 10% beyond the introduced razor cut, at which point fracturing at the crack tip was assumed independent of any effects of the initial cutting. When 10% growth was observed, the number of cycles needed for the crack to grow an additional 10% of its current length was estimated (200–25 000 cycles). These cycles were applied, and crack length was then re-measured. This process was iterated until the crack stopped growing or the sample broke in two.

For each crack-length measurement, crack growth rate, *da/dN,* was estimated as increase in crack length between measurements, Δa, divided by the number of cycles between measurements, ΔN. Also for each measurement, strain energy release rate, T_S, was calculated as was done for rubber (e.g. Seldén, 1995):

$$T_s = \frac{2\pi W_{o,S}\left(\frac{a_1+a_2}{2}\right)}{\sqrt{1+\epsilon_{max}}} , \quad (7)$$

with $W_{o,S}$ determined as a function of cycle number from Eqn 6, a_1 the crack length at the beginning of the interval, a_2 the crack length at the end of the interval, and ϵ_{max} the maximum strain imposed on the sample in each cycle [see eqn 9 in accompanying article (Mach et al., 2007)]. Again, the subscript 'S' indicates that T is calculated from *stored* strain energy density. This equation resembles Eqn 2, used for pull-to-break tests, with the substitution of an average measure of crack length.

Several precautions minimized the time required for measurement of crack length, during which loading stopped. First, crack length was measured at a relatively infrequent rate, only after the crack was estimated to have grown by 10%, as was done for rubber (Seldén, 1995). And second, tank draining and subsequent measurement of crack length were completed as rapidly as possible.

Predictions of lifetime

Fatigue lifetime, as a function of maximum cyclic stress, was calculated for *P. occidentalis*, *U. expansa*, and *M. flaccida* using a crack-growth-based approach. An empirically determined power-law function was used to describe the relationship between energy release rate, T_S, and crack growth rate, *da/dN*, during repeated-loading tests (Lake, 1995; Seldén, 1995) [see eqn 16 in accompanying article (Mach et al., 2007)]:

$$\frac{da}{dN} = B T_S^{\beta} = B\left(\frac{2\pi W_{o,S} a}{\sqrt{1+\epsilon_{max}}}\right)^{\beta}, \quad (8)$$

where B and β are constants measured for a species. Rearranging and then integrating this equation yields predicted fatigue lifetime, N_f, the number of cycles until fracture of an un-notched sample (Lake, 1995; Seldén, 1995) [see eqn 17 in accompanying article (Mach et al., 2007)]:

$$N_f = \frac{1}{(\beta-1)B\left(\frac{2\pi W_{o,S,cyclic\sigma}}{\sqrt{1+\epsilon_{cyclic\sigma}}}\right)^{\beta}}\left(\frac{1}{a_o^{\beta-1}} - \frac{1}{a_C^{\beta-1}}\right), \quad (9)$$

where a_o is again the effective size of cracks assumed to occur naturally in the test piece, and a_C is critical crack length, the crack size at which complete fracture of the sample occurs, given as:

$$a_C = \frac{T_{C,S}\sqrt{1+\epsilon_{cyclic\sigma}}}{2\pi W_{o,S,cyclic\sigma}} , \quad (10)$$

where average $T_{C,S}$ for each species was determined from

Eqn 2. Values of strain, $\epsilon_{cyclic\sigma}$, and stored strain energy density, $W_{o,S,cyclic\sigma}$, were determined as functions of cyclically applied stress by subjecting rectangular test pieces to 25 cycles between zero strain and a given maximum, beginning at maximum strain of 0.10. Maximum strain was increased by 5% after each 25-cycle test until the sample broke. For the last cycle at each maximum strain level, maximum stress and maximum stored strain energy density were determined. Polynomials were then fit to these data to find maximum cyclic strain and stored strain energy density as functions of maximum cyclic stress. The number of cycles required for an assumed, naturally occurring crack in a sample to grow to failure could then be estimated from Eqn 9.

For each species, several values of B and β were used in Eqn 9 to indicate the range of fatigue lifetimes predicted from crack growth data. B and β were first calculated from all experimental data for each species. For *M. flaccida*, fatigue lifetimes were also determined for 'upper-bound' values of B and β, and for *U. expansa*, B and β determined for a subset of the species' data were used to exclude effects of an outlying crack-growth-rate point. Finally, fatigue lifetimes were calculated for each species using B and β values calculated from the combined data of all species.

To relate our results to flow conditions in the field, we calculated approximate water velocities corresponding to experimentally applied stresses for a *M. flaccida* frond. Of species in this study, *M. flaccida* is the only one for which drag coefficients are available, and it is generally exposed to the greatest wave forces in the field. Drag coefficients from Bell (Bell, 1992) were used to determine drag force and thus stress as a function of wave-imposed water velocities. As we show below, *M. flaccida* is predicted to accumulate fatigue damage for stresses imposed by water velocities greater than approximately 8 m s^{-1}.

This estimated water-velocity threshold for fatigue damage was used to approximate time (rather than number of cycles) to failure. Based on continuous wave force measurements at Hopkins Marine Station (M. L. Boller and M. J. O'Donnell, personal communication), we found that 5% of waves are associated with intertidal water velocities greater than 8 m s^{-1} on a day of average offshore significant wave height (1.0 m). Given a wave period of 10 s, we then estimated that water velocities exceed 8 m s^{-1} every 200 s, on average. Thus, a cycle of loading that causes fatigue damage will occur every 200 s. This approximation likely overestimates the rate of imposition of water velocities over 8 m s^{-1} because some small wave-induced forces, below the sensitivity limit of measurement devices, were not recorded and because intertidal seaweeds are not exposed to waves for the entirety of each day.

Results

Single-edge-notch, pull-to-break tests

A representative example of critical-strain-energy-release-rate calculation is shown in Fig. 4, and values for all species are listed in Table 1. Resilience as a function of strain (Eqn 2 and Eqn 3) is given in Table 2. Initial effective crack length, a_o, was calculated from Eqn 4 as 0.25 mm for *Mazzaella flaccida* and 0.31 mm for *Ulva expansa*. For *Porphyra occidentalis*, a_o was not determined owing to the large variation in values of $T_{C,S}$ and to the difficulty of producing fracture away from the grips in un-notched specimens. For use in subsequent calculations, a_o for *P. occidentalis* was set to 0.28 mm, the average a_o for *M. flaccida* and *U. expansa* combined.

Fig. 5 depicts calculated breaking stresses as functions of

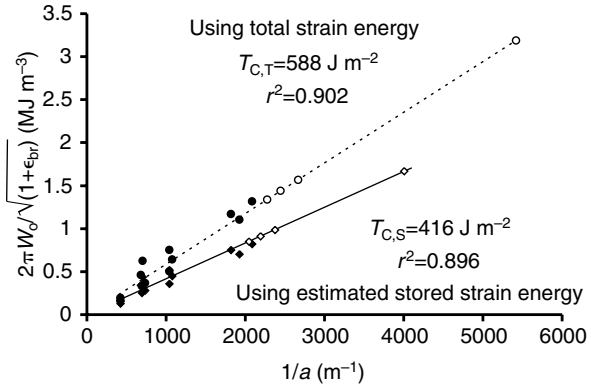

Fig. 4. An example of calculating critical strain energy release rate, T_C, for *M. flaccida* in single-edge-notch, pull-to-break tests. The inverse of crack length, a, introduced into each sample is plotted against $(2\pi W_o a)/(\sqrt{1+\epsilon_{br}})$ at fracture, where W_o is calculated as total absorbed strain energy density, $W_{o,T}$, and estimated stored strain energy density, $W_{o,S}$. Solid circles indicate data points calculated from total strain energy density; solid diamonds indicate data points calculated from stored strain energy density. T_C is the slope of the regression line for each data set: regression line (broken line) for data points calculated from total strain energy density yields an estimate of $T_{C,T}$, and regression line (solid line) for data points calculated from estimated stored strain energy density yields an estimate of $T_{C,S}$, as defined in the text. Open circles and diamonds indicate data points for un-notched samples, for which effective crack length was estimated.

Table 1. *Critical strain energy release rate calculated through several tests and relations*

	SEN		SEN cyclic
	$T_{C,T}$, Eqn 1	$T_{C,S}$, Eqn 2	$T_{C,S}$
Mazzaella flaccida	588±40	416±25	452±88
Porphyra occidentalis	853±202	581±139	417±203
Ulva expansa	238±27	113±17	158

T_C, critical strain energy release rate (J m^{-2}), calculated from total absorbed strain energy density (Eqn 1) and from stored strain energy density (Eqn 2).

SEN, single-edge-notch pull-to-break tests. SEN cyclic T_C values from repeatedly loaded SEN samples were calculated from stored strain energy density as described in the text.

Values are mean ± s.e.m. (N=?), except for *U. expansa*, where only one sample displayed crack growth to fracture in the SEN, repeated-loading tests.

Table 2. *Resilience determined as a function of strain*

	Resilience=L_1+L_2 × strain		
	L_1	L_2	r^2
Mazzaella flaccida	0.965	–0.722	0.991
Porphyra occidentalis	1.207	–1.422	0.999
Ulva expansa	0.568	–1.090	0.861

r^2 values were derived from linear regressions. Correlation for *P. occidentalis* is for strain greater than 0.20; for this species, resilience cannot be calculated for lower strains using the equation given.

crack size (Eqn 5) along with measured breaking stresses determined in single-edge-notch, pull-to-break tests. Breaking stress showed the most predictable correlation with crack length for *M. flaccida* specimens and demonstrated poor correlation with crack length for *P. occidentalis*. Because of the high variability in critical strain energy release rate for *P. occidentalis*, we show predicted lower bounds of breaking stress for different crack lengths (Fig. 5B), using the consistent lower-bound values of $T_{C,S}$ and $T_{C,T}$ in Eqn 5.

For blades with notches less than 0.5 mm in length, *U. expansa* blades are expected to break at the lowest stresses, and *P. occidentalis* blades are predicted to break at the highest stresses. Few data points are given for un-notched blades (on the ordinate) due the difficulty of producing fracture away from the grips. Actual breaking stresses for un-notched blades are probably greater than values shown here, especially for *P. occidentalis* and *U. expansa*, because stronger specimens were more likely to fail at the grips first.

Crack propagation in single-edge-notch, repeated-loading tests

In single-edge-notch tests involving repeated cycling, maximum stored strain energy density, $W_{o,S}$, in each cycle decreased during conditioning cycles, before crack introduction; a representative example is depicted in Fig. 6. The majority of decrease in strain energy density occurred during the first 50 cycles, but further decrease continued throughout the conditioning period and was considered for each sample with Eqn 6. *U. expansa*, the only green alga in the study, showed greater decrease in strain energy density than the red algae *M. flaccida* and *P. occidentalis*.

Growth of an introduced crack in a *M. flaccida* sample, occurring over more than 60 000 loading cycles, is depicted in Fig. 7. This representative plot demonstrates that crack growth rate, *da/dN*, varies over the course of crack growth. When the crack was first introduced, the sharpness of the crack tip resulted in rapid initial crack growth. Once the initial crack tip blunted, crack growth slowed. When crack length increased by 10% from its initial value, crack growth rate was assumed independent of initial effects of razor-blade nicking, and further data collected were used in crack growth analyses. Crack growth became increasingly rapid as specimen fracture was approached.

Measured crack growth rates for all cycled specimens are plotted as functions of energy release rate in Fig. 8A. Critical energy release rates, $T_{C,S}$, were estimated from these plots (Table 1). In addition, the strain energy release rate below which crack growth did not occur, T_o, was estimated as 100 J m^{-2} for *M. flaccida*, 35 J m^{-2} for *P. occidentalis*, and 70 J m^{-2} for *U. expansa*. Stable crack growth was extremely

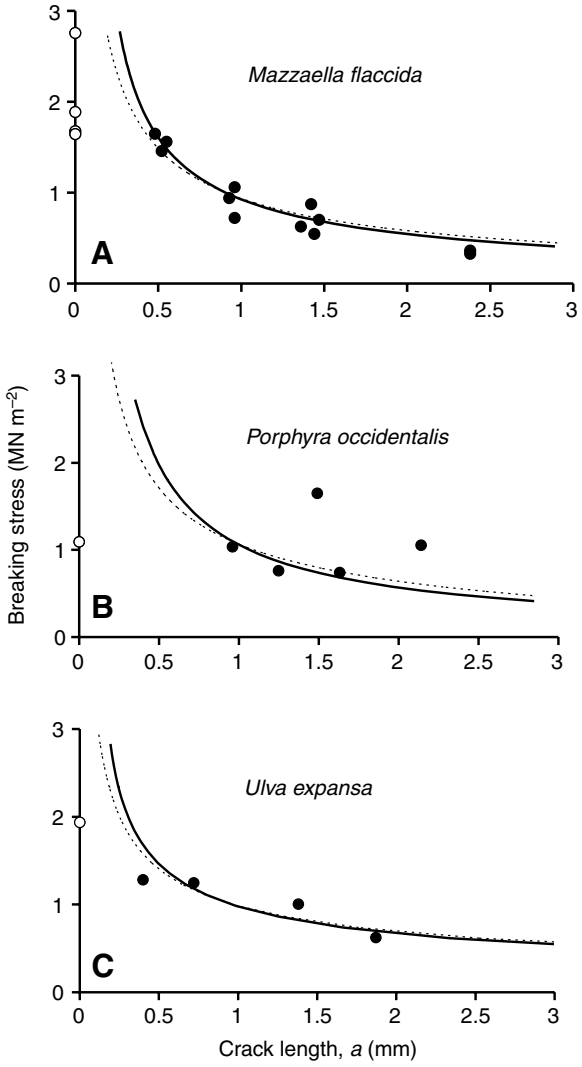

Fig. 5. Measured and predicted breaking stresses as a function of crack length, *a*, for (A) *M. flaccida*, (B) *P. occidentalis* and (C) *U. expansa*. In each plot, data points indicate breaking stress measured as a function of crack length in single-edge-notch, pull-to-break tests. Data points on ordinate (open circles) are for un-notched test pieces. Solid line indicates predicted breaking stress as determined from Eqn 5 using critical strain energy release rate calculated from estimated stored strain energy density. Broken line indicates predicted breaking stress based on critical strain energy release rate calculated from total strain energy density. Curve equations are as follows, with breaking stress in units of MPa and crack length, *a*, in m: (A) solid line: breaking stress=$3510a^{-0.81}$, r^2=0.933; broken line: breaking stress=$9530a^{-0.66}$, r^2=0.935; (B) solid line: breaking stress=$2123a^{-0.90}$, r^2=0.0033; broken line: breaking stress=$8668a^{-0.69}$, r^2=0.0030; (C) solid line: breaking stress=$17650a^{-0.58}$, r^2=0.712; broken line: breaking stress=$28790a^{-0.51}$, r^2=0.724.

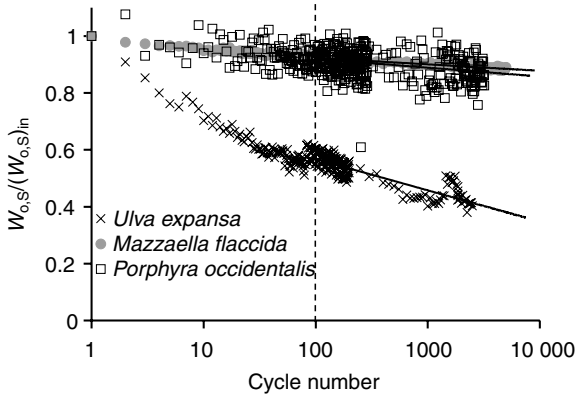

Fig. 6. Reduction in maximum strain energy density per cycle during the conditioning period for three algal species used in this study. $W_{o,S}/(W_{o,S})_{in}$ is the ratio of maximum stored strain energy density in a given cycle to maximum stored strain energy density of the initial cycle for that specimen. The abscissa is on a log scale. Solid lines represent regressions calculated excluding data from the first 100 cycles.

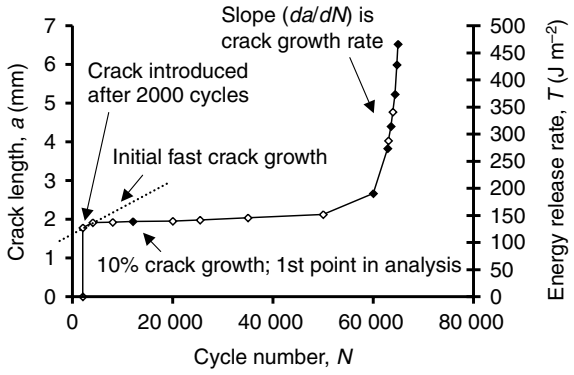

Fig. 7. An example of crack growth in a single-edge-notch specimen for cyclic repeated loading at 1 Hz to 0.166 strain. Approximate energy release rate as a function of crack size, calculated as if change in strain energy density with cycling (Eqn 6) were negligible, is shown on the secondary ordinate. Only data points for which crack growth was equal to or greater than 10% of previously used value (filled points) were used in analysis of crack growth rate.

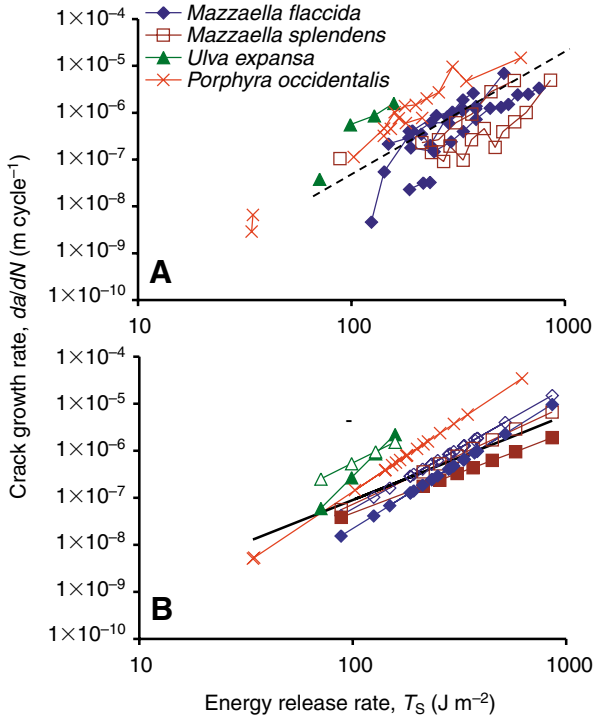

Fig. 8. Empirical (A) and calculated (B) fatigue crack growth rates (m cycle^{-1}), *da/dN*, plotted against energy release rate (J m^{-2}), T_S, in single-edge-notch, repeatedly loaded test pieces. Axes in plots are logarithmic. Data for test specimens that did not demonstrate crack growth are not shown. In both A and B, diamonds represent *M. flaccida*, squares, *M. splendens*, triangles, *U. expansa*, and crosses, *P. occidentalis*. Symbols used in A are given in the plot. For B, the black line with no symbols represents the power-law series for all data collected for all species. Again in B, solid symbols (diamonds, squares, triangles, and crosses) represent power-law series calculated from all data for each species. Open diamonds (*M. flaccida*) and squares (*M. splendens*) are for relations determined from the upper bounds of crack growth rates for the two species. Open triangles are for a relation for *U. expansa* that excludes the lowest crack growth rate point for *U. expansa* in A.

difficult to produce in *U. expansa* blades; most cracks did not grow or else fractured after only a few cycles following razor cutting.

Predictions of lifetime

Crack-growth power-law functions (Eqn 8) were determined from plots of *T versus da/dN* (Fig. 8A). B and β for the different species' power-law functions are given in Table 3, and crack growth rates predicted from these power-law functions are shown in Fig. 8B. As depicted in Fig. 8A, noticeable variation occurred in measures of crack growth rate. One source of this variation was branching of the crack tip, which caused cracks to propagate more slowly. For *M. flaccida* and *M. splendens*, for which the variation was most substantial, an upper bound on crack growth rate for each species was thus determined. The upper bound for *M. flaccida* is shown as the broken line in Fig. 8A. In determining power-law functions to describe crack growth rates (Eqn 8), points along the upper bound of plots of *T versus da/dN*, were arbitrarily selected for *M. flaccida* and *splendens*, to supplement power-law functions determined for these species overall. No r^2 values are given for the upper-bound *M. splendens* and *flaccida* relations in Table 3 since regression points were arbitrarily selected. In addition, two power-law functions were determined for *U. expansa*, with an outlying data point that suggests an exceptionally low initial crack growth rate excluded for the second relation.

Fig. 9 depicts cycles to failure in terms of each repeatedly applied stress's percent of breaking strength, as calculated from Eqn 9. (Breaking strength is estimated stress at fracture for un-notched specimens in pull-to-break tests.) Values of B and β for Eqn 9 are given in Table 3, and polynomials for Eqn 9 that

Table 3. *Fatigue crack growth parameters for examined species*

	Eqn 8, $da/dN=BT_S^{\beta}$		
	B	β	r^2
Mazzaella flaccida			
All	4.84×10^{-14}	2.83	0.641
Upper bound	4.04×10^{-13}	2.58	–
Mazzaella splendens			
All	1.81×10^{-11}	1.71	0.490
Upper bound	4.57×10^{-12}	2.10	–
Porphyra occidentalis			
All	1.12×10^{-13}	3.04	0.957
Ulva expansa			
All	2.60×10^{-16}	4.52	0.897
Excluding outlier	1.82×10^{-11}	2.24	0.976
Overall	2.27×10^{-11}	1.80	0.452

These measured constants, B and β, are used in Eqn 8 to describe crack growth rate as a function of energy release rate. T_S is in J m^{-2}, and *da/dN* in m cycle^{-1}.

Parameters for each species were determined from all data for that species ('All' parameters), and the 'Overall' parameters were calculated from crack growth data collected for all species. For *M. flaccida* and *splendens*, crack growth parameters were also determined for data along an upper bound. The second set of parameters for *U. expansa* excludes a low crack-growth-rate data point that contributed disproportionately to parameters determined from all of the *U. expansa* data.

relate maximum strain, $\epsilon_{cyclic\sigma}$, and maximum stored strain energy density, $W_{o,S,cyclic\sigma}$, to maximum cyclic stress are listed in Table 4.

Fig. 10 depicts loading cycles to failure as a function of repeatedly applied stress for *M. flaccida*, the only species with known drag coefficients.

For Figs 9 and 10, curves are broken for cyclically applied loading stresses that correspond to energy release rates below the fatigue threshold, T_o, for unnotched specimens. The repeatedly applied stress below which cracks of length a_o will not propagate was estimated as 0.7 MN m^{-2} for *U. expansa*, 0.7 MN m^{-2} for *M. flaccida*, and 0.3 MN m^{-2} for *P. occidentalis*. *U. expansa* blades are predicted to display no crack growth at stresses less than 75% of pull-to-break strength (Fig. 9C), while *P. occidentalis*, at the other extreme, is predicted to fail eventually at stresses only 10% of its pull-to-break strength (Fig. 9B). *M. flaccida* is predicted to accumulate fatigue damage due to stresses imposed by water velocities greater than approximately 8 m s^{-1} (Fig. 10). Figs 9 and 10 indicate the number of cycles required for failure by fatigue cracking: *M. flaccida* may fail in fewer than 10 000 loadings, *P. occidentalis* may fail in fewer than 30 000 loadings, and *U. expansa* may fail in fewer than 3000 loadings. The secondary ordinates in Figs 9 and 10 represent lower-bound estimates of time to failure and indicate that all three species may fail by fatigue in hours or days.

Crack propagation rates in Figs 9 and 10 are maximum rates that assume cracks propagate as single sharp cracks. Power-law

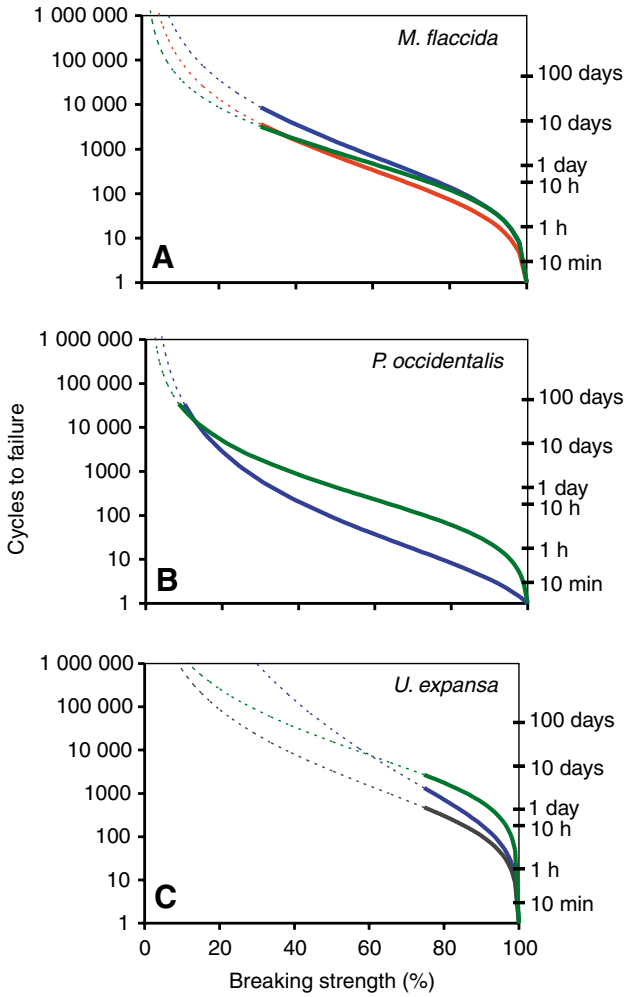

Fig. 9. Fatigue lifetime curves depicting predicted cycles to fracture as a function of percent of breaking strength. Blue curves are calculated from parameters for all data for a given species ('All' in Table 3), green curves are determined from parameters for all algal data combined ('Overall' in Table 3), red curve is for the upper-bound parameters for *M. flaccida* ('Upper Bound' in Table 3), and gray curve is for *U. expansa* parameters determined excluding an outlying data point ('Excluding Outlier' in Table 3). Broken portions of curves are below measured fatigue thresholds, T_o, for which no crack growth is predicted. An approximate time to failure is given on the secondary ordinate. As described in the text, time to failure is calculated assuming that each wave has a period of 10 s and that approximately 1 in 20 waves imposes stresses great enough to cause fatigue damage.

functions describing crack growth (Eqn 8, Table 3) were calculated for samples that did not display substantial bifurcation of growing cracks or peeling apart of blade cell layers.

Discussion

Critical energy release rate calculations

For measurements of critical strain energy release rate (Table 1), coefficients of variation for *Mazzaella flaccida* and

Table 4. *Polynomials (for Eqn 9 and Eqn 10) describing maximum cyclic strain and corresponding maximum strain energy density as a function of maximum cyclic stress*

		$Y=M_0+M_1\sigma_{max}+M_2\sigma_{max}^2+M_3\sigma_{max}^3+M_4\sigma_{max}^4$					
Alga	Y variable	M_0	M_1	M_2	M_3	M_4	r^2
Mazzaella flaccida	$\epsilon_{cyclic\sigma}$	0.0190	5.32×10^{-7}	-2.52×10^{-13}	5.04×10^{-20}	0	0.99
	$W_{o,S,cyclic\sigma}$	–1433	0.0923	2.19×10^{-8}	1.03×10^{-14}	0	0.99
Porphyra occidentalis	$\epsilon_{cyclic\sigma}$	0.0439	6.83×10^{-7}	-3.88×10^{-13}	0	0	0.99
	$W_{o,S,cyclic\sigma}$	–2714	0.0722	3.166×10^{-8}	0	0	0.99
Ulva expansa	$\epsilon_{cyclic\sigma}$	5.80×10^{-3}	2.91×10^{-7}	-2.15×10^{-13}	1.12×10^{-19}	-2.11×10^{-26}	0.99
	$W_{o,S,cyclic\sigma}$	–157.8	0.0174	5.27×10^{-8}	0	0	0.99

$\epsilon_{cyclic\sigma}$, maximum cyclic strain, and $W_{o,S,cyclic\sigma}$, corresponding maximum strain energy density (J m^{-3}), as a function of σ_{max}, maximum cyclic stress (Pa).

$\epsilon_{cyclic\sigma}$ for *P. occidentalis* was calculated as a piecewise function. The given polynomial is replaced by $\epsilon_{cyclic\sigma}=0.115+3.33\times10^{-7}\sigma_{max}$ for $\sigma_{max}>550\,000$ Pa.

Ulva expansa T_C values are consistent with T_C coefficients of variation determined for rubber (Nakajima and Liu, 1993) and bone (Currey, 1998), materials for which fracture mechanics has been used successfully to characterize structural integrity. Only variation in *Porphyra occidentalis* T_C exceeds published values for other biological and soft materials.

Calculations of T_C using stored strain energy density (Table 1) are likely more accurate than calculations from total strain energy density because stored strain energy density excludes energy dissipated within a specimen, which is included in total strain energy density but does not contribute to crack elongation.

Cracks were introduced using razor blades, and specimen fracture in pull-to-break tests proceeded directly from the resulting sharp crack tips. Sharpness of these crack tips likely resulted in fracture at lower stresses than if the crack tips had more natural, somewhat rounded geometries. The initially high crack growth rates observed in repeatedly loaded, single-edge-notch test specimens also indicate the greater ease with which sharp, razor-introduced cracks propagate, but these initial high growth rates were excluded from analyses.

Biological implications

Variability in calculated critical strain energy release rates may indicate that different parts of algal blades vary in their susceptibility to crack propagation. This variability may help explain tattering in marginal regions of thalli, which avoids more catastrophic breakage (e.g. Blanchette, 1997), or may affect dispersal if reproductive portions of blades are more prone to tearing. Furthermore, holes found in blades, especially common in *U. expansa*, may slow the overall course of crack growth by providing gaps that must be bridged or bypassed by growing cracks. T_C values were lowest for *U. expansa*, indicating that blades of this species may be the most susceptible to fracture. It is worth noting that healthy *U. expansa*, in addition to growing on rocks and docks, is often found floating freely in protected areas (Abbot and Hollenberg, 1976). Thus, a tear propagating across an entire blade may be less lethal for *U. expansa* than for *P. occidentalis* and *M. flaccida*.

Critical strain energy release rate, breaking stress and strain energy density measurements throughout this study were least variable for *M. flaccida*, perhaps due to the cellular composition of its blades or to wave action it experiences in the field. *M. flaccida* blades are thicker than *P. occidentalis* and *U. expansa* blades, with more medullary tissue, which may behave as a more homogenous material than the closely packed cell layers of *P. occidentalis* and *U. expansa*. However, it is worth noting that cell size in all studied species is small (cell diameters of approximately 0.01 mm) compared to lengths of introduced cracks. In addition, of the three species, *M. flaccida* is exposed to the greatest wave-induced forces in the field, which may select over evolutionary time or among blades in a population for more uniformly robust material performance.

Critical energy release rates measured in this study are similar to values measured for other algae and biological materials (Biedka et al., 1987; Denny et al., 1989) (Table 5).

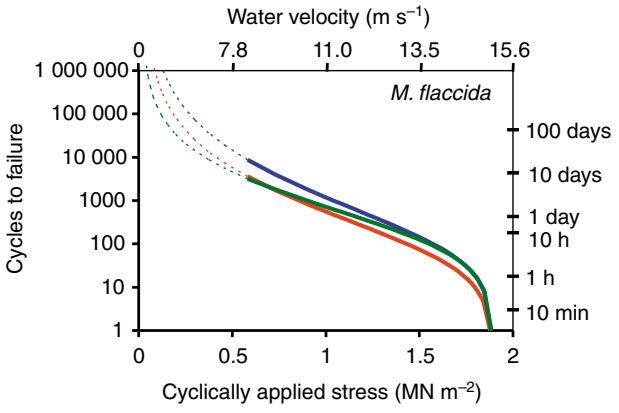

Fig. 10. Fatigue lifetime curves depicting predicted cycles to fracture as a function of cyclic stress for *M. flaccida*. Broken portions of curves are below measured fatigue threshold, T_o, for which no crack growth is predicted. Color-coding of curves is as described for Fig. 9. Approximate water velocities corresponding to applied stresses are given on the secondary abscissa. Estimated time to failure, determined as described in the text, is given on the secondary ordinate.

Table 5. *Critical energy release rates for various materials*

Material	T_C (J m^{-2})
Horse hoof keratin (in tension)	5200–13 500[A]
Bone (in tension)	400–2900[B]
Grasses (in tension)	850–21 650[C]
From trouser tear and tensile tests, as noted in legend:	
Zostera marina blade (L)	256[D]
Laminaria setchellii blade (T)	740[D]
Laminaria setchellii blade (L)	2420[D]
Egregia menziesii blade	556[D]
Silvetia compressa blade	684[D]
Fucus gardneri blade	572[D]
Cystoseira osmundacea blade	396[D]
Rhodymenia pacifica blade	816[D]
Prionitis lanceolata blade	832[D]
Mastocarpus papillatus blade	936[D]
Gastroclonium subarticulatum blade	336[D]
Mazzaella flaccida blade	556[D], 416[E]
Porphyra occidentalis blade	581[E]
Ulva expansa blade	113[E]
Pterygophora californica stipe (T)	830[F]
Pterygophora californica stipe (L)	1646[F]

T_C, critical energy release rate.

Transverse (T) and longitudinal (L) fracture, across and along grain, is specified in some cases. Correction factors used to make energy release rates equivalent: [A](Bertram and Gosline, 1986); [B](Currey, 1998); [C](Vincent, 1991); [D](Denny et al., 1989), from trouser tear tests, values multiplied by 4; [E]this study, values from Eqn 2; [F](Biedka et al., 1987), from trouser tear tests, values multiplied by 2.

Note that critical strain energy release rates calculated by Bertram and Gosline (Bertram and Gosline, 1986) involve techniques from elastic-plastic fracture mechanics and are reported as J_C rather than T_C [see accompanying article (Mach et al., 2007)]. Also, critical strain energy release rates calculated by Currey (Currey, 1998) and Vincent (Vincent, 1991) involve techniques from linear elastic fracture mechanics and are more nearly G_C than T_C [see accompanying article (Mach et al., 2007)].

Fatigue lifetime predictions

Our results suggest that fatigue may play an important role in breakage of marine algae. For all species studied, imposed stresses well below breaking strength are predicted to cause fracture within hours or days (Figs 9 and 10). The potential importance of fatigue processes in wave-swept macroalgae has long been suggested, and these results provide the first evidence that fatigue crack growth is indeed relevant to seaweeds.

Previous comparisons of algal pull-to-break strengths and maximal field stresses have predicted that, contrary to observation, seaweeds should rarely break. Perhaps rectifying these discrepancies between prediction and reality, this study indicates that wave-induced stresses may break seaweeds commonly, not in single pull-to-break loadings, but due to the accumulated effects of repeated stressing.

Our estimates of fatigue lifetimes, based on numbers of cycles required for crack growth to fracture in un-notched blades, require several qualifications. First, and most importantly, fatigue lifetimes as estimated here assume that initial, 'effective' cracks in un-notched samples grow similarly to longer cracks observed in this study. However, crack growth may deviate from the power-law functions used here when cracks are very small. In addition, the fatigue lifetime curves in Fig. 9 predict that any blade containing a propagating crack subjected to repeated loading will resist cycling indefinitely or fracture within 30 000 cycles. However, some specimens in the single-edge-notch, repeated-loading tests fractured after many more than 30 000 cycles (e.g. Fig. 7). But in other single-edge-notch, repeated-loading tests, cracks slowed or stopped propagating, perhaps due to cracks encountering deformities in blades or due to single propagating cracks branching into two or more cracks.

Fracture mechanics estimates of lifetime are statistical predictions that cannot predict the exact fates of individual plants. Variability among individuals stemmed from unknown prior loading histories and from the variable nature of fracture and fatigue processes. Although blade samples used in this study had no macroscopic damage, they were collected from the field, where they had undergone unknown numbers of wave force loadings and had potentially accumulated some level of fatigue damage prior to testing. Fracture parameters and lifetime calculations were determined accordingly for algae of average fatigue damage, not for specimens with known pre-experiment loading histories. Thus, predictions made with techniques outlined here are applicable as averages for given populations. Nonetheless, our primary conclusion stands: fatigue crack growth may cause failure of wave-swept algae under conditions in which imposition of a single stress would not cause breakage.

Our predictions of fatigue lifetimes do not consider biological repair. Although a certain number of cycles at high stress may cause blade fracture (Figs 9 and 10), if these high-stress cycles are separated by low-stress cycles that do not cause crack propagation, algae may have time to repair fractured tissues or round crack tips in a way that mitigates subsequent crack growth. In addition, the energy release rate below which crack growth does not occur may be effectively increased through tissue repair.

In this study, standard loading protocols involving sinusoidal variation in strain were used to explore application of fracture mechanics to macroalgal crack growth. Subsequent studies could evaluate several aspects of loading protocol that may be important in comparing field and laboratory crack growth. First, the rate of strain energy input from waves or laboratory loading – with rate calculated per unit time or per loading cycle – may influence crack growth rates. Second, different strain rates and waveforms during each loading may change crack growth rates. Third, viscoelastic changes as well as biological repair, potentially acting over different time scales, may occur during loading stoppages, possibly altering the course of crack growth.

We emphasize, however, that standard laboratory loading protocols have successfully characterized naturally variable

fatigue processes in rubbers even though typical loading regimes are invariably more complex for these materials (e.g. Lake, 1995; Seldén, 1995). Simplified laboratory testing of engineering materials is adequate to predict field performance, and indeed for seaweeds, more elaborate testing methods may not improve accuracy of predictions, in light of inherent variability in fatigue processes. Most field loadings on algal blades in this study can be modeled as drag forces imposed in tension, and the sinusoidal, tensile cyclic loadings we have used to study crack growth approximate field stresses as has been done for engineering materials.

For future studies, we note that algal blades represent particularly good model organisms for investigating crack growth and repair because blades are often naturally planar, easily kept alive in seawater, and frequently only one or two cells thick, all of which make crack tips and new tissue growth easily observable.

Conclusion

Although subsequent experiments should probe additional aspects of fracture and fatigue, the results reported here demonstrate that failure through fatigue crack growth may be an important component of life for wave-swept macroalgae, with breakage resulting from repeated imposition of small stresses. Fatigue processes may have similar consequences for any biological structure subjected to repeated loads.

List of symbols and abbreviations

The equation in which each symbol is first used is given (if it is used in an equation).

a	measure of crack length, Eqn 1
a_C	critical crack length, Eqn 9
a_o	initial (effective) crack length, Eqn 4
a_1	initial crack length, Eqn 7
a_2	final crack length, Eqn 7
B	fitted constant, Eqn 8
C_1	fitted constant, Eqn 6
C_2	fitted constant, Eqn 6
da/dN	crack growth rate, Eqn 8
k	specimen extension parameter
N	cycle number, Eqn 6
N_f	fatigue lifetime, Eqn 9
R	resilience, Eqn 3
SEN	single-edge-notch
T	strain energy release rate
T_C	critical strain energy release rate
$T_{C,S}$	critical strain energy release rate calculated from $W_{o,S}$, Eqn 2
$T_{C,T}$	critical strain energy release rate calculated from $W_{o,T}$, Eqn 1
T_o	threshold strain energy release rate
T_S	strain energy release rate calculated from $W_{o,S}$, Eqn 7
W_o	strain energy density
$W_{o,S}$	stored (recoverable) strain energy density, Eqn 2
$W_{o,S,cyclic\sigma}$	$W_{o,S}$ as a function of maximum cyclically applied stress, Eqn 9
$W_{o,S,\sigma}$	$W_{o,S}$ as a function of applied stress, Eqn 5
$W_{o,T}$	total absorbed strain energy density, Eqn 1
$W_{o,T,\sigma}$	$W_{o,T}$ as a function of applied stress, Eqn 5
β	fitted constant, Eqn 8
ϵ	strain
ϵ_{br}	breaking strain, Eqn 1
$\epsilon_{cyclic\sigma}$	strain as a function of maximum cyclically applied stress, Eqn 9
ϵ_{max}	maximum strain in a cycle, Eqn 7
ϵ_σ	strain as a function of applied stress, Eqn 5
σ	applied stress in bulk of specimen
σ_{max}	maximum stress in a cycle

This manuscript benefited from the suggestions and insights of M. Boller, J. Gosline, B. Grone, L. Hunt, J. Mach, P. Martone, K. Miklasz, L. Miller, and two anonymous reviewers. NSF grants OCE 9633070 and OCE 9985946 to M. Denny supported this research.

References

Abbot, I. A. and Hollenberg, G. J. (1976). *Marine Algae of California*. Stanford, CA: Stanford University Press.

Ahagon, A., Gent, A. N., Kim, H. J. and Kumagai, Y. (1975). Fracture energy of elastomers in mode I (cleavage) and mode III (lateral shear). *Rubber Chem. Technol.* **48**, 896-901.

Armstrong, S. L. (1987). Mechanical properties of the tissues of the brown alga *Hedophyllum sessile* (C. Ag.) Setchell: variability with habitat. *J. Exp. Mar. Biol. Ecol.* **114**, 143-151.

Bell, E. C. (1992). Consequences of morphological variation in an intertidal macroalga: physical constraints on growth and survival of *Mastocarpus papillatus* Kützing. PhD thesis, Stanford University, USA.

Bertram, J. E. A. and Gosline, J. M. (1986). Fracture toughness design in horse hoof keratin. *J. Exp. Biol.* **125**, 29-47.

Biedka, R. F., Gosline, J. M. and DeWreede, R. E. (1987). Biomechanical analysis of wave-induced mortality in the marine alga *Pterygophora californica*. *Mar. Ecol. Prog. Ser.* **36**, 163-170.

Black, R. (1976). The effects of grazing by the limpet, *Acmaea insessa*, on the kelp, *Egregia laevigata*, in the intertidal zone. *Ecology* **57**, 265-277.

Blanchette, C. A. (1997). Size and survival of intertidal plants in response to wave action: a case study with *Fucus gardneri*. *Ecology* **78**, 1563-1578.

Broek, D. (1982). *Elementary Engineering Fracture Mechanics*. Boston: Martinus Nijhoff Publishers.

Busfield, J. J. C., Jha, V., Liang, H., Papadopoulos, I. C. and Thomas, A. G. (2005). Prediction of fatigue crack growth using finite element analysis techniques applied to three-dimensional elastomeric components. *Plast. Rubber Compos.* **34**, 349-356.

Carew, E. O., Garg, A., Barber, J. E. and Vesely, I. (2004). Stress relaxation preconditioning of porcine aortic valves. *Ann. Biomed. Eng.* **32**, 563-572.

Carrington, E. (1990). Drag and dislodgment of an intertidal macroalga: consequences of morphological variation in *Mastocarpus papillatus* Kützing. *J. Exp. Mar. Biol. Ecol.* **139**, 185-200.

Connell, J. H. (1978). Diversity in tropical rain forests and coral reefs. *Science* **199**, 1302-1310.

Currey, J. D. (1998). Mechanical properties of vertebrate hard tissues. *Proc. Inst. Mech. Eng.* **212**, 399-411.

Denny, M. W. (2006). Ocean waves, nearshore ecology, and natural selection. *Aquatic Ecol.* **40**, 439-461.

Denny, M. and Gaylord, B. (2002). The mechanics of wave-swept algae. *J. Exp. Biol.* **205**, 1355-1362.

Denny, M., Brown, V., Carrington, E., Kraemer, G. and Miller, A. (1989). Fracture mechanics and the survival of wave-swept macroalgae. *J. Exp. Mar. Biol. Ecol.* **127**, 211-228.

Denny, M. W., Gaylord, B. P. and Cowen, E. A. (1997). Flow and flexibility:

II. The roles of size and shape in determining wave forces on the bull kelp *Nereocystis luetkeana*. *J. Exp. Biol.* **200**, 3165-3183.

DeWreede, R. E., Ewanchuk, P. and Shaughnessy, F. (1992). Wounding, healing and survivorship in three kelp species. *Mar. Ecol. Prog. Ser.* **82**, 259-266.

Dorfmann, A. and Ogden, R. W. (2004). A constitutive model for the Mullins effect with permanent set in particle-reinforced rubber. *Int. J. Solids Struct.* **41**, 1855-1878.

Dorfmann, A., Trimmer, B. A. and Woods, W. A. (2007). A constitutive model for muscle properties in a soft-bodied arthropod. *J. R. Soc. Interface* **4**, 257-269.

Dudgeon, S. R. and Johnson, A. S. (1992). Thick vs. thin: thallus morphology and tissue mechanics influence differential drag and dislodgment of two co-dominant seaweeds. *J. Exp. Mar. Biol. Ecol.* **165**, 23-43.

Dudgeon, S. R., Steneck, R. S., Davison, I. R. and Vadas, R. L. (1999). Coexistence of similar species in a space-limited intertidal zone. *Ecol. Monogr.* **69**, 331-352.

Edsberg, L. E., Mates, R. E., Baier, R. E. and Lauren, M. (1999). Mechanical characteristics of human skin subjected to static versus cyclic normal pressures. *J. Rehabil. Res. Dev.* **36**, 133-141.

Emery, J. L., Omens, J. H. and McCulloch, A. D. (1997). Strain softening in rat left ventricular myocardium. *J. Biomech. Eng.* **119**, 6-12.

Franceschini, G., Bigoni, D., Regitnig, P. and Holzapfel, G. A. (2006). Brain tissue deforms similarly to filled elastomers and follows consolidation theory. *J. Mech. Phys. Solids* **54**, 2592-2620.

Friedland, M. T. and Denny, M. W. (1995). Surviving hydrodynamic forces in a wave-swept environment: consequences of morphology in the feather boa kelp, *Egregia menziesii* (Turner). *J. Exp. Mar. Biol. Ecol.* **190**, 109-133.

Gaylord, B. (2000). Biological implications of surf-zone flow complexity. *Limnol. Oceanogr.* **45**, 174-188.

Gaylord, B., Blanchette, C. A. and Denny, M. W. (1994). Mechanical consequences of size in wave-swept algae. *Ecol. Monogr.* **64**, 287-313.

Gaylord, B., Hale, B. B. and Denny, M. W. (2001). Consequences of transient fluid forces for compliant benthic organisms. *J. Exp. Biol.* **204**, 1347-1360.

Holbrook, N. M., Denny, M. W. and Koehl, M. A. R. (1991). Intertidal 'trees': consequences of aggregation on the mechanical and photosynthetic properties of sea-palms *Postelsia palmaeformis* Ruprecht. *J. Exp. Mar. Biol. Ecol.* **146**, 39-67.

Janssen, M., Zuidema, J. and Wanhill, R. J. H. (2004). *Fracture Mechanics* (2nd edn). London: Spon Press.

Johnson, A. S. (2001). Drag, drafting, and mechanical interactions in canopies of the red alga *Chondrus crispus*. *Biol. Bull.* **201**, 126-135.

Johnson, A. S. and Koehl, M. A. R. (1994). Maintenance of dynamic strain similarity and environmental stress factor in different flow habitats: thallus allometry and material properties of a giant kelp. *J. Exp. Biol.* **195**, 381-410.

Johnson, C. R. and Mann, K. H. (1986). The importance of plant defence abilities to the structure of subtidal seaweed communities: the kelp *Laminaria longicruris* de la Pylaie survives grazing by the snail *Lacuna vincta* (Montagu) at high population densities. *J. Exp. Biol. Mar. Ecol.* **97**, 231-267.

Kadir, A. and Thomas, A. G. (1984). Tearing of unvulcanized natural rubber. *J. Polym. Sci. Polym. Phys. Ed.* **22**, 1623-1634.

Kinloch, A. J. and Young, R. J. (1983). *Fracture Behaviour of Polymers*. London: Applied Science Publishers.

Kitzes, J. A. and Denny, M. W. (2005). Red algae respond to waves: morphological and mechanical variation in *Mastocarpus papillatus* along a gradient of force. *Biol. Bull.* **208**, 114-119.

Koehl, M. A. R. (1984). How do benthic organisms withstand moving water? *Am. Zool.* **24**, 57-70.

Koehl, M. A. R. (1986). Seaweeds in moving water: form and mechanical function. In *On the Economy of Plant Form and Function* (ed. T. J. Givnish), pp. 603-634. Cambridge: Cambridge University Press.

Koehl, M. A. R. and Alberte, R. S. (1988). Flow, flapping, and photosynthesis of *Nereocystis luetkeana*: a functional comparison of undulate and flat blade morphologies. *Mar. Biol.* **99**, 435-444.

Lake, G. J. (1983). Aspects of fatigue and fracture of rubber. *Prog. Rubber Technol.* **45**, 89-143.

Lake, G. J. (1995). Fatigue and fracture of elastomers. *Rubber Chem. Technol.* **68**, 435-460.

Leigh, E. G., Paine, R. T., Quinn, J. F. and Suchanek, T. H. (1987). Wave energy and intertidal productivity. *Proc. Natl. Acad. Sci. USA* **84**, 1314-1318.

Lowell, R. B., Markham, J. H. and Mann, K. H. (1991). Herbivore-like damage induces increased strength and toughness in a seaweed. *Proc. R. Soc. Lond. B Biol. Sci.* **243**, 31-38.

Mach, K. J., Nelson, D. V. and Denny, M. W. (2007). Techniques for predicting the lifetimes of wave-swept macroalgae: a primer on fracture mechanics and crack growth. *J. Exp. Biol.* **210**, 2213-2230.

Mars, W. V. and Fatemi, A. (2004). Observations of the constitutive response and characterization of filled natural rubber under monotonic and cyclic multiaxial stress states. *J. Eng. Mater. Technol.* **126**, 19-28.

Martone, P. T. (2006). Size, strength and allometry of joints in the articulated coralline *Calliarthron*. *J. Exp. Biol.* **209**, 1678-1689.

Meguid, S. A. (1989). *Engineering Fracture Mechanics*. London: Elsevier Applied Science.

Mullins, L. (1969). Softening of rubber by deformation. *Rubber Chem. Technol.* **42**, 339-362.

Nakajima, N. and Liu, J. L. (1993). Fracture toughness of PVC/NBR blends evaluated by the *J*-Integral. *Rubber Chem. Technol.* **66**, 634-645.

Pratt, M. C. and Johnson, A. S. (2002). Strength, drag, and dislodgment of two competing intertidal algae from two wave exposures and four seasons. *J. Exp. Mar. Biol. Ecol.* **272**, 71-101.

Rivlin, R. S. and Thomas, A. G. (1953). Rupture of rubber. I. Characteristic energy for tearing. *J. Polym. Sci.* **10**, 291-318.

Seldén, R. (1995). Fracture mechanics analysis of fatigue of rubber – a review. *Prog. Ser. Rubber Plast. Technol.* **11**, 56-83.

Seymour, R. J., Tegner, M. J., Dayton, P. K. and Parnell, P. E. (1989). Storm wave induced mortality of giant kelp, *Macrocystis pyrifera*, in Southern California. *Estuar. Coast. Shelf Sci.* **28**, 277-292.

Smith, S. V. and Kinsey, D. W. (1976). Calcium carbonate production, coral reef growth, and sea level change. *Science* **194**, 937-939.

Utter, B. D. and Denny, M. W. (1996). Wave-induced forces on the giant kelp *Macrocystis pyrifera* (Agardh): field test of a computational model. *J. Exp. Biol.* **199**, 2645-2654.

Vincent, J. F. V. (1991). Strength and fracture of grasses. *J. Mater. Sci.* **26**, 1947-1950.

Wainwright, S. A., Biggs, W. D., Currey, J. D. and Gosline, J. M. (1976). *Mechanical Design in Organisms*. New York: J. Wiley.